

Accelerating Mobile Edge Generation (MEG) by Constrained Learning

Xiaoxia Xu, *Member, IEEE*, Yuanwei Liu, *Fellow, IEEE*, Xidong Mu, *Member, IEEE*, Hong Xing, *Member, IEEE*, Arumugam Nallanathan, *Fellow, IEEE*

Abstract

A novel accelerated mobile edge generation (MEG) framework is proposed for generating high-resolution images on mobile devices. Exploiting a large-scale latent diffusion model (LDM) distributed across edge server (ES) and user equipment (UE), cost-efficient artificial intelligence generated content (AIGC) is achieved by transmitting low-dimensional features between ES and UE. To reduce overheads of both distributed computations and transmissions, a dynamic diffusion and feature merging scheme is conceived. By jointly optimizing the denoising steps and feature merging ratio, the image generation quality is maximized subject to latency and energy consumption constraints. To address this problem and tailor LDM sub-models, a low-complexity MEG acceleration protocol is developed. Particularly, a backbone meta-architecture is trained via offline distillation. Then, dynamic diffusion and feature merging are determined in online channel environment, which can be viewed as a constrained Markov Decision Process (MDP). A constrained variational policy optimization (CVPO) based MEG algorithm is further proposed for constraint-guaranteed learning, namely MEG-CVPO. Numerical results verify that: 1) The proposed framework can generate 1024×1024 high-quality images over noisy channels while reducing over 40% latency compared to conventional generation schemes. 2) The developed MEG-CVPO effectively mitigates constraint violations, thus flexibly controlling the trade-off between image distortion and generation costs.

Index Terms

Artificial intelligence generated content (AIGC), edge artificial intelligence (AI), generative AI (GAI), mobile edge generation (MEG), reinforcement learning (RL).

X. Xu, Y. Liu, X. Mu, and A. Nallanathan are with the School of Electronic Engineering and Computer Science, Queen Mary University of London, London E1 4NS, U.K. (email: {x.xiaoxia, yuanwei.liu, xidong.mu, a.nallanathan}@qmul.ac.uk).

H. Xing is with the Internet of Things Thrust, The Hong Kong University of Science and Technology (Guangzhou), Guangzhou 511400, China (email: hongxing@ust.hk).

I. INTRODUCTION

Over the recent years, artificial intelligence generative content (AIGC) has emerged as a transformative technology to autonomously create diverse vivid contents ranging between images, videos, and music, thus revolutionizing the digital economy and information society. Leveraging the power of large-scale Generative Artificial Intelligence (GAI) models such as ChatGPT [1], Stable Diffusion, and DALL-E [2], the high-fidelity contents generated by AIGC services have presented superior qualities comparable to human artefacts. The autonomous and manipulable content creations and modifications can significantly reduce the man-power costs and time overheads, which have shown huge economic values [3]. Driven by the burgeoning downstream digital applications of AIGC and the vision of connected intelligence, enabling AIGC on mobile devices, e.g., smartphones, has attracted increasing attentions [4]. Interconnected with wireless radios, the on-device AIGC services provided by intelligent mobile networks are promising to support intensive service access, ubiquitous human-machine interactions, and improved user experiences [5].

Due to the restricted computing and storage capacities of mobile devices [6], the large-scale GAI models with billions of parameters and extensive computations are typically deployed on high-performance cloud computing servers. However, the remote nature of cloud services results in high latency, which limits the application and proliferation of AIGC services on mobile applications. To reduce the latency in accessing mobile AIGC services, mobile edge generation (MEG) [7] has been recently proposed as a promising solution for developing centralized generative models toward edge AI. The key idea is to enable distributed and scalable AIGC capabilities across multiple computation nodes in mobile edge networks, which provides the following appealing benefits:

- MEG decomposes the sophisticated large-scale GAI models into distributed sub-models deployed at user equipment (UE) and the nearby edge server (ES), respectively. By jointly executing the distributed sub-models, the edge resources can be fully exploited.
- In conventional centralized generation, the server-generated contents need to be transmitted to the UE, which may lead to leakage of sensitive and personal information, and cause excessive service latency for high-resolution image or video generation. In MEG, the ES and UE only needs to exchange low-dimensional features extracted by distributed GAI sub-models, which can reduce the transmission latency and preserve user privacy.

- The GAI sub-model deployed at the UE can be customized for personalized applications and individual purposes, thus facilitating the personalization of AIGC services.
- In addition, efficient training and inference of GAI models can be supported by the beyond fifth-generation (B5G) and the sixth-generation (6G) techniques with massive connectivity, low latency, and bit-beyond transmissions.

Given the above attractive benefits, MEG will contribute to the development and user experience improvement for mobile AIGC services. To pave the way toward cost-efficient, latency-sensitive, and energy-constrained on-device AIGC, this paper investigates the solution to accelerate MEG processing and unleash its potentials.

A. Related Works

1) *Related Works on Edge AI*: MEG can be regarded as a customized edge AI solution for AIGC services. In previous works, extensive research efforts have been devoted to edge AI for mobile deep neural networks (DNNs) applications, mainly including *edge inference* and *device-edge co-inference* [8]. Specifically, *edge inference* deploys DNNs on edge servers in close proximity to mobile devices [9], [10], thus avoiding the high latency for routing data to the cloud and achieving fast inference. Nevertheless, uploading large-volume data such as 3D images and high-resolution videos still results in a high transmission latency, which is intolerable for real-time mobile DNN applications. To combat this drawback, the *device-edge co-inference* has been considered as another promising option [8], [11], which harnesses distributed computing resources across both ES and mobile devices to reduce the transmission overheads. The *device-edge co-inference* can be simply implemented by splitting a pre-trained DNN into separate sub-models and deploys them over the ES and UE, respectively [12]. To further achieve feature compression for co-inference, a learning-based communication scheme was proposed in [13] to jointly optimize feature extraction, source coding, and channel coding. Based on information bottleneck framework [14], a variational feature compression method was developed to adaptively identify and prune redundant neurons of the encoded features. By integrating joint source-channel coding (JSCC), the authors of [15] jointly optimized the feature pruning and encoding in an end-to-end framework for image classification.

2) *Related Works on Mobile AIGC*: To support AIGC services at mobile edge networks, the authors of [4] conceived a collaborative cloud and edge infrastructure. By performing AIGC model pre-training at cloud server and offloading content generation to edge devices, low-latency

and personalized AIGC services can be achieved. To overcome limited resources and unstable channels, a semantic communication empowered AIGC generation and transmission framework was proposed in [5] to adjust edge and local computations. In [7], the authors introduced the concept of MEG and proposed various distributed deployment schemes for GAI models, thus reducing the user queueing latency in accessing GAI services. Furthermore, the authors of [16] proposed a novel diagram of MEG enabled digital twins and conceived single-user and multi-user generation mechanisms. Considering a multi-user collaborative diffusion model in wireless networks, the authors of [17] proposed a user-centric interactive AI method. By sharing several denoising steps for users with semantically similar prompts, energy constraints can be ensured while maximizing users' quality of experience (QoE). To deal with limited bandwidth resources and dynamic channels at mobile edge networks, a pricing-based incentive mechanism was developed in [18] for AIGC generation and transmission, thus maximizing the utility of users. Furthermore, focusing on the security aspects, the authors of [19] proposed a novel paradigm named TrustGAIN to deliver trustworthy AIGC services in 6G networks, which can efficiently defend against malicious or fake messages.

B. Motivations and Contributions

Previous studies have laid a solid foundation on the training and inference of sophisticated AI models at mobile edge networks. However, effective MEG architectures and resource-constrained solutions for low-latency on-device generation are still less explored currently. Due to the fundamental trade-off between content generative quality and resource limitations, there are several crucial challenges to meet intensive AIGC service requests and accelerate MEG:

- The newly emerging GAI techniques (e.g., diffusion model (DM) and Transformer) rely on tailored compression schemes at mobile edge networks to reduce the end-to-end generation latency, which requires different designs compared to conventional DNNs such as multi-layer perceptron (MLP) and convolutional neural networks (CNN).
- To reduce transmission overheads, conventional edge AI typically exploits neuron pruning to compress transmitted features for classification/regression. However, the generation qualities of AIGC are very sensitive to neuron pruning, particularly for high-resolution data such as image and video streams. To achieve low-latency generation, effective feature compression strategies should be investigated for MEG.

- Current GAI model compression techniques mainly exploit manually configured hyper-parameters for computational acceleration and ignore transmission overheads. However, the on-device generation should satisfy end-to-end latency and energy consumption constraints specific to channel conditions in an online edge environment. To enable controllable distortion-latency trade-off, efficient constrained learning methods are required for dynamic end-to-end acceleration of MEG.

To address the aforementioned issues, we propose a novel accelerated MEG framework for high-resolution image generation in this paper. The proposed framework distributes the large-scale GAI model, i.e., latent diffusion model (LDM), across both the ES and the UE. To accelerate joint execution of distributed sub-models, a dynamic diffusion and feature merging scheme is proposed, which achieves few-step diffusion and length-adaptive transmitted features to relieve computation and communication overheads, respectively. Different from conventional pruning-based feature transmission schemes that discard information of pruned neurons, the proposed scheme merges similar neurons to construct low-dimensional features, thereby retaining image content details. Our goal is to maximize the image generation quality while satisfying latency and energy consumption constraints. This is formulated as a high-complexity non-convex optimization problem, where the objective function is a black-box function without explicit mathematical modelling. To make it tractable, a low-complexity dynamic MEG acceleration protocol is devised. A backbone meta-architecture is first learned via offline distillation. Then, the denoising steps and feature merging ratios are dynamically determined in the online prediction by solving a constrained Markov Decision process (MDP). To achieve constrained learning for MEG acceleration, we further develop a constrained variational policy optimization (CVPO) based MEG algorithm, namely MEG-CVPO. The proposed MEG-CVPO algorithm can improve the dynamic policy over a trusted region that results in feasible action distributions. Our main contributions can be summarized as follows.

- We propose a novel accelerated MEG framework, which enables cost-efficient on-device generation of high-resolution images via a large-scale LDM distributed across the UE and the nearby ES. By jointly optimizing the denoising steps and feature merging ratios, the generation quality is maximized subject to both latency and energy constraints.
- We develop a low-complexity protocol for dynamic MEG acceleration. The designed protocol first learns a meta-architecture via offline distillation. Based on the meta-architecture,

on-demand dynamic diffusion and feature merging can be realized in online channel environment. This recasts the formulated problem as a constrained MDP.

- We propose a constrained reinforcement learning (RL) algorithm for MEG by invoking the CVPO theory, namely MEG-CVPO. Relying on the variational inference, the policy is trained to improve system rewards while achieving feasible action distributions. This effectively mitigates constraint violations and solves the constrained MDP.
- We provide numerical results to verify the effectiveness. Compared to conventional generative schemes, the proposed dynamic diffusion and feature merging scheme can reconstruct high-quality 1024×1024 images over noisy channels within $3 \sim 8$ seconds, which realizes over 40% latency reduction compared to conventional generation schemes. Furthermore, the MEG-CVPO algorithm effectively mitigates constraint guarantees compared to conventional Lagrangian-based learning methods, thereby striking a controllable trade-off between generation quality and costs.

C. Organization and Notation

The rest of this paper is organized as follows. Section II presents the accelerated MEG framework and formulates the image generation quality maximization problem. In Section III, a low-complexity protocol for dynamic compression is designed. Furthermore, a constrained MEG-CVPO learning algorithm is developed in Section IV to achieve dynamic diffusion and feature merging solutions. Section V provides numerical results to verify efficiencies of the proposed MEG framework, and Section VI finally concludes the paper.

Notation: Vectors and matrices are denoted by bold-face letters. $\lfloor x \rfloor$ indicates the rounding operation of value x . $\|\mathbf{x}\|$ denotes the Euclidean norm of a vector \mathbf{x} .

II. SYSTEM MODEL AND PROBLEM FORMULATION

A. Framework for MEG Acceleration

To enable real-time AI content generation on mobile devices, we propose an accelerated MEG framework empowered by edge intelligence environment, as shown in Fig. 1. Specifically, the MEG framework consists of an ES equipped with a high-performance computing platform, which communicates with a low-cost UE to offer mobile AIGC services for real-time applications. The generation tasks are sequentially submitted by the UE to the ES, which will be served in T time frames, indexed by $\mathcal{T} = \{1, 2, \dots, T\}$. Due to the limited computational power and scarce memory

of mobile terminal, it is generally difficult for the UE to handle the overwhelming computation burdens required by GAI model. To address this challenge, MEG decomposes the original GAI model into two associated sub-models, including a large-scale sub-model deployed at the ES and a tiny sub-model at the UE, respectively. Therefore, AIGC services can be fulfilled by jointly and collaboratively executing the decomposed sub-models. Upon receiving the generation service requests from the UE, the ES first performs smart computations based on high-complexity DNNs, e.g., self-attention Transformers, via powerful graphics processing units (GPUs). Then, important features from the immediate results can be extracted and encoded into low-dimensional features, which are sent to the UE through the noisy wireless channels. By decoding the received features, the UE further performs high-quality content generation locally via lightweight computations.

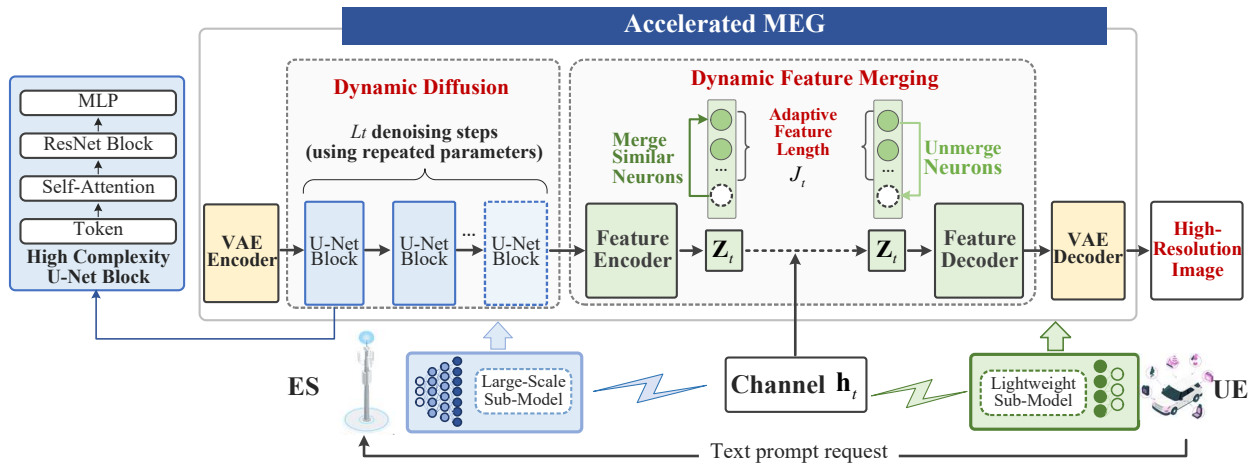


Fig. 1: The proposed dynamic MEG acceleration framework.

To accelerate on-device generation in the mobile edge environment, a crucial aspect is the cost-effective compression of both large-scale GAI sub-models and transmitted features. To this end, we propose a novel dynamic compression structure at mobile edge networks for LDM, which is one of the most popular GAI models in current AIGC applications for text-to-image and image-to-image generations. We focus on text-to-image generation in this work. As shown in Fig. 1, a standard LDM typically includes three components, i.e., a VAE encoder, a denoising diffuser based on U-Net [20], and a VAE decoder. Since each U-Net block includes multiple high-complexity self-attention Transformer layers and ResNet layers, the denoising diffusion process usually results in high computational loads and delays. Considering limited computing resources of UE, we deploy the high-complexity VAE encoder and U-Net denoising diffuser at

the ES and the lightweight VAE decoder at the UE, respectively. After receiving the text prompts from users, the ES-side sub-model encodes and denoises the latent features via the VAE encoder and denoising diffuser, respectively. By transmitting the extracted latent features to the UE, high-resolution images are then decoded by the VAE decoder. Therefore, the intensive computations of LDM can be achieved by collaborative inference of ES and UE.

As the ES and the UE only exchanging low-dimensional latent features instead of the high-dimensional raw images, the joint execution of distributed sub-models can reduce the service latency compared to conventional centralized generation schemes. Nevertheless, the denoising diffuser at ES usually requires a time-consuming complex reverse diffusion process, which repeatedly executes a U-Net block for tens of denoising steps to maintain performance [21], [22]. Furthermore, the latent features extracted by the ES-side sub-model need to be transmitted through noisy channels to the UE-side for image decoding, which still results in communication burdens and quality degradation. To reduce computational and transmission burdens, our proposed compression structure enables a dynamic reverse diffusion process for fast acceleration and a variable-length feature merging for efficient transmissions.

- **Dynamic Diffusion:** We define L_{\max} as the maximal number of denoising steps at the denoising diffuser, which reuses the U-Net block parameters to execute self-attention and convolutional operations, thus denoising and extracting the latent features for content generation. We define an accelerating ratio $\alpha_t \in [0, 1]$ to decide the diffusion process acceleration at each time frame t , where only $L_t = \lfloor \alpha_t L_{\max} \rfloor$ denoising steps will be performed for relieving the computational burdens.
- **Feature Merging:** Given generation task g_t , the ES exploits the VAE encoder and dynamic reverse diffusion process to obtain the latent feature $\mathbf{Z}_t^O = [\mathbf{z}_{1,t}^O, \mathbf{z}_{2,t}^O, \dots, \mathbf{z}_{J_{\max},t}^O] \in \mathbb{R}^{d^C \times J_{\max}}$. Moreover, d^C and J_{\max} denote the original channel number and length of the feature extracted by the ES-side sub-model, respectively. The latent feature will be transmitted from the ES to the UE to perform on-device high-quality content generation. To reduce feature transmission overheads and latency specific to the system environment states, we develop a novel feature merging scheme to adaptively decrease the feature length. Specifically, by flexibly determining the merging ratio β_t at each time frame, $\lfloor \beta_t J_{\max} \rfloor$ neurons will be trimmed out and their information will be merged into the remaining neurons. This leads to a length-adaptive feature $\mathbf{Z}_t \in \mathbb{R}^{d^C \times J_t}$ with length $J_t = J_{\max} - \lfloor \beta_t J_{\max} \rfloor$.

The detailed implementations of the dynamic diffusion and feature merging will be discussed in Section III-A.

B. Performance Modelling

1) *Latency Model*: At each time frame t , the ES will fetch a generation task request g_t from the buffer q_t . Newly arrival tasks will be stored in the task buffer during the processing of task g_t . The tasks in the buffer will be served during each time frame in a first-in first-out (FIFO) manner. As shown in Fig. 2, given the input $\mathbf{X}_t \in \mathbb{R}^{1 \times d^{\text{in}}}$ of task G_t , the end-to-end latency for completing a generation task mainly includes the following three parts, i.e., computation latency, transmission latency, and queuing latency.

- **Computation latency**: The computation latency at ES is decided by floating point operations (FLOPs) of the VAE encoder, the U-Net denoiser, and the denoising steps, i.e.,

$$D_t^{\text{ES}} = \frac{O^{\text{E}} + \lfloor \alpha_t L_{\text{max}} \rfloor O^{\text{UNet}}}{f^{\text{ES}}}, \quad (1)$$

where O^{E} and O^{UNet} indicate the required FLOPs for computing the VAE encoder and a single U-Net block, respectively. Moreover, f^{ES} is the floating point operation per second (FLOPS) of ES's GPU that measures the data processing speed. Furthermore, the computation latency at UE can be given by

$$D_t^{\text{UE}} = O^{\text{D}} / f^{\text{UE}}, \quad (2)$$

where O^{D} denotes the FLOPs of VAE decoder and f^{UE} is the FLOPS of UEs' computational processor.

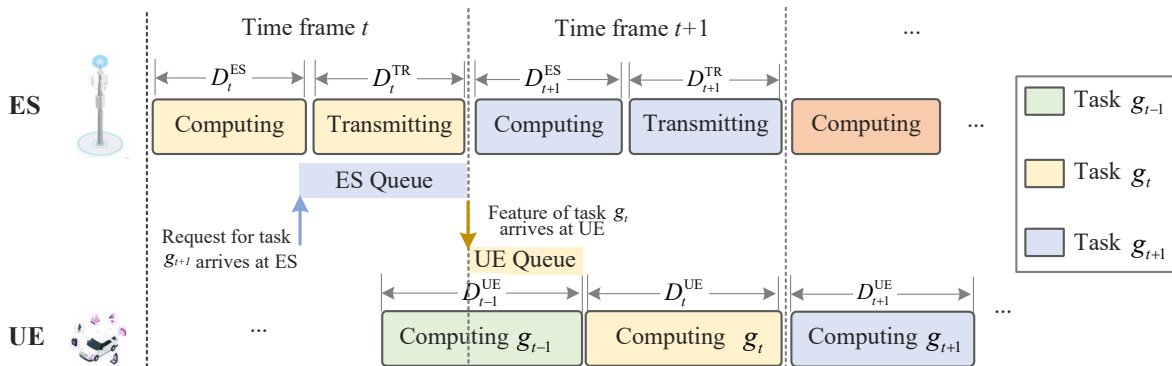


Fig. 2: A diagram of latency model for MEG.

- **Transmission latency:** The transmission latency depends on both the size of the transmitted feature and the channel gain of UE. Hence, the transmission latency can be modelled by

$$D_t^{\text{TR}} = \frac{bd^{\text{C}}(J_{\max} - \lfloor \beta_t J_{\max} \rfloor + J_t^{\text{aux}})}{B_0 \log_2 \left(1 + \frac{P_0 h_t}{N_0} \right)}, \quad (3)$$

where h_t denotes the UE's channel gain at time frame t , b is the number of bits of each floating number, and B_0 indicates the bandwidth of each resource block (RB). P_0 denotes the downlink transmit power of the ES, and N_0 is the additive white Gaussian noise (AWGN). Moreover, J_t^{aux} represents the overheads of additional information required to be transmitted to UE in order to keep the dimensional consistency between the feature and the UE-side sub-model. For feature pruning, UE can acquire the neuron importance in advance and pad the pruned neurons with zero values, which leads to $J_t^{\text{aux}} = 0$. In comparison, as feature merging is task-specific, an additional information overhead $J_t^{\text{aux}} = 1/d^{\text{C}} \times \lfloor \beta_t J_{\max} \rfloor$ is required to inform UE which dimensions the pruned neurons have been merged into, and thereby enable the feature unmerging at UE.

- **Queueing latency:** The queueing latency includes both the ES-side queueing and the UE-side queueing. Note that the duration of each time frame t can be denoted by $\Delta_t = D_t^{\text{ES}} + D_t^{\text{TR}}$. Then, the ES-side queueing delay of generation task g_t can be defined as $D_t^{\text{Q-ES}} = \varrho_{g,t-1} \Delta_{t-1}$, where $\varrho_{g,t-1}$ is the fraction of time task g_t arrives at the ES in time frame $(t-1)$. Furthermore, the UE-side queueing delay of the task batch \mathcal{G}_t can be given by $D_t^{\text{Q-UE}} = \Omega_t / f^{\text{UE}}$, with $\Omega_{g,t}$ being the required FLOPs for remaining computation tasks at the UE when it obtains the encoded features for generation task g_t in time frame t . Therefore, the queueing latency of task batch \mathcal{G}_t can be computed by

$$D_t^{\text{Q}}(\Delta_{t-1}, \Omega_{g,t}) = \varrho_{g,t-1} \Delta_{t-1} + \frac{\Omega_t}{f^{\text{UE}}}. \quad (4)$$

Combining the above definitions, the end-to-end generation latency can be modelled by

$$D_t^{\text{E2E}}(\beta_t, \alpha_t) = D_t^{\text{ES}} + D_t^{\text{UE}} + D_t^{\text{TR}} + D_t^{\text{Q}}(\Delta_{t-1}). \quad (5)$$

2) *Energy Consumption Model:* For completing the generation task g_t , the computing energy consumption at the ES and UE using the proposed MEG framework can be represented by

$$E_t(\beta_t, \alpha_t) = E_t^{\text{ES}}(\alpha_t^{\text{ES}}) + E_t^{\text{TR}}(\beta_t) + E_t^{\text{UE}}, \quad (6)$$

where $E_t^{\text{ES}}(\alpha_t)$ and E_t^{UE} indicate ES-side and UE-side computation energy consumption, respectively, and $E^{\text{TR}}(\beta_t)$ indicates the energy consumption for transmitting encoded features. The computational energy consumption can be estimated by model FLOPS and the energy efficiency of the computing hardware [23]. Based on our proposed framework, the computational energy consumption can be given by

$$E_t^{\text{ES}}(\alpha_t^{\text{ES}}) = \frac{O^{\text{E}} + \lfloor \alpha_t L_{\max} \rfloor O^{\text{UNet}}}{\eta^{\text{ES}}}, \quad (7)$$

where η^{ES} denotes the energy efficiency of ES computing, i.e., the energy dissipations for each float-operation point computation. Meanwhile, the energy consumption to transmit the encoded feature \mathbf{Z}_t between ES and UE can be denoted by

$$E_t^{\text{TR}}(\beta_t) = P_0 D_{g,t}^{\text{TR}} = \frac{P_0 b d^{\text{C}} (J_{\max} - \lfloor \beta_t J_{\max} \rfloor + J_t^{\text{aux}})}{B_0 \log_2 \left(1 + \frac{P_0 h_t}{B_0 N_0} \right)}. \quad (8)$$

C. Problem Formulation

Based on the proposed framework, the generated contents \mathbf{Y}_t can be expressed as a function of the diffusion accelerating ratio α_t , feature merging ratio β_t , ES-side sub-model $\mathcal{F}^{\text{E}}(\cdot)$ for feature encoding, and UE-side sub-model $\mathcal{F}^{\text{D}}(\cdot)$ for feature decoding, i.e.,

$$\mathbf{Y}_t = \mathcal{Y}_t(\alpha_t, \beta_t, \mathcal{F}^{\text{E}}(\cdot), \mathcal{F}^{\text{D}}(\cdot) \mid \mathbf{X}_t, h_t, \Omega_t, \Delta_{t-1}). \quad (9)$$

Therefore, we can formulate the dynamic compression optimization problem for accelerating MEG under limited latency and energy consumption. Our goal is to maximize the content generative qualities $f_{\text{G}}(\mathbf{Y}_t \mid \mathbf{X}_t, h_t, \Omega_t, \Delta_{t-1})$, $t = 1, 2, \dots, T$, by jointly optimizing the diffusion accelerating ratio, feature merging ratio, and GAI sub-models, subject to the end-to-end latency and energy consumption constraints. Mathematically, we have

$$\mathcal{P}_0 : \max_{\alpha_t, \beta_t, \mathcal{F}^{\text{E}}(\cdot), \mathcal{F}^{\text{D}}(\cdot)} \frac{1}{T} \sum_{t \in \mathcal{T}} f_{\text{G}}(\mathbf{Y}_t \mid \mathbf{X}_t, h_t, \Omega_t, \Delta_{t-1}) \quad (10a)$$

$$\text{s.t. C1 : } \frac{1}{T} \sum_{t=1}^T D_t^{\text{E2E}}(\beta_t, \alpha_t) \leq D_{\max}, \quad (10b)$$

$$\text{C2 : } \frac{1}{T} \sum_{t=1}^T (E_t^{\text{UE}}(\beta_t, \alpha_t) + E_t^{\text{ES}}(\beta_t, \alpha_t)) \leq E_{\max}, \quad (10c)$$

$$\text{C3 : } 0 \leq \alpha_t, \beta_t \leq 1, \quad \forall t \in \mathcal{T}. \quad (10d)$$

While problem \mathcal{P}_0 striking a trade-off between generation quality and latency, there are several difficulties to search for the optimal solutions. First, the highly non-convex length-adaptive neuron merging and dynamic diffusion is an NP-hard problem. Moreover, the objective function $f_G(\cdot)$ and the latency constraint have unknown modelling and dynamics, whose mathematical models are difficult to be obtained. Additionally, it is non-trivial to achieve on-demand MEG acceleration as well as ensuring latency/energy constraints specific to real-time channels and system states in the online environment. This renders the inapplicability and infeasibility of conventional mathematical optimization theory. To meet this challenges, we will develop a low-complexity learning-driven protocol in the following section.

III. LOW-COMPLEXITY PROTOCOL FOR DYNAMIC MEG ACCELERATION

In this section, we present a low-complexity learning-driven protocol for dynamic MEG acceleration. Note that it is extremely challenging to jointly train billions of sub-model parameters while optimizing the denoising steps and feature merging ratio in \mathcal{P}_0 . Therefore, we decouple the customization of sub-models and the optimization of dynamic acceleration into two consecutive stages, i.e., offline distillation and online prediction. Specifically, the offline distillation trains a cost-efficient meta-architecture to approximate the performance of the centralized GAI model, thus efficiently exploiting few-step diffusions and dimension-reduced transmitting features, as well as overcome channel noises. This can establish a backbone architecture for online prediction and reduce the search space. Relying on this meta-architecture, the online prediction further achieves on-demand compression and dynamic acceleration of GAI models specific to real-time channels and task features, which can be modelled as constrained MDP.

A. Few-Step Diffusion and Feature Merging Designs

1) *Few-Step Diffusion Distillation*: LDM performs a forward noise addition process and a reverse denoising diffusion process over the latent feature $\mathbf{Z}_t^{(0)}$ that is extracted by the VAE encoder at time frame t . During the forward diffusion, the latent feature $\mathbf{Z}_t^{(0)}$ is corrupted by Gaussian noises step by step. The noise-corrupted feature at noise addition step l is given by

$$\mathbf{Z}_t^{(l)} = \sqrt{1 - \sigma_{\text{diff}}^2(l)}\mathbf{Z}_t^{(0)} + \sigma_{\text{diff}}(l)\epsilon, \quad l = 1, 2, \dots, L_{\text{max}}, \quad (11)$$

where ϵ and σ_{diff}^2 denote the random Gaussian noises and the variance, respectively. Then, during the reverse denoising diffusion process, the denoising diffuser learns to recover $\mathbf{Z}_t^{(0)}$ from $\mathbf{Z}_t^{(L_{\text{max}})}$

by repeatedly executing U-Net in denoising steps $L_{\max}, L_{\max} - 1, \dots, 0$. To achieve fast denoising diffusion, DDIM has been proposed to efficiently solve the probability flow ordinary differential equations (ODEs) based on their semi-linear structures. Nevertheless, DDIM still requires tens of denoising steps to maintain the generation quality, which are time-consuming for mobile generation. To overcome this limitation, we distill the high-cost denoising diffusion process into the few-step denoising diffusion through the offline distillation. To train a backbone denoising diffuser that is applicable to variable denoising steps, we identify an effective distillation technique, namely rectified flow [26]. Rectified flow utilizes linear interpolation to reconstruct the target distribution φ_0 of desired feature $\mathbf{Z}_t^{(0)}$ from the noise distribution φ_l of corrupted feature $\mathbf{Z}_t^{(l)}$ at each step l . The few-step diffusion and the original ODE solver are known as student model and teacher model, respectively. The student diffusion model learns a noise prediction neural network $\epsilon_{\varpi}(\mathbf{Z}_t^{(l)}, l)$, parameterized by ϖ , to predict noise at each denoising step l , thus transporting the noise-corrupted feature $\mathbf{Z}_t^{(l)} \sim \varphi_l$ into the target feature $\mathbf{Z}_t^{(l-1)} \sim \varphi_{l-1}$. Given denoising steps L , we create L time windows, where the l -th time window $[\tau_l, \tau_{l-1})$ is given by a starting point τ_l and an end point τ_{l-1} , respectively. For each time window l , the target feature $\mathbf{Z}_t^{(l)} \sim \varphi_{l-1}$ is constructed by the ODE solver $\Phi(\mathbf{Z}_t^{(l)}, \tau_l, \tau_{l-1})$. Using $\epsilon_{\varpi}(\mathbf{Z}_t^{(l)}, l)$, the denoised feature is given by

$$\mathbf{Z}_t^{(l-1)} = \vartheta_k \mathbf{Z}_t^{(l)} + \varrho_l \epsilon_{\varpi}(\mathbf{Z}_t^{(l)}, l), \quad (12)$$

where parameters ϑ_k and ϱ_l balance between current states and estimated noises. We have $\vartheta_k = \sqrt{v_{l-1}/v_l}$ and $\varrho_l = \sqrt{1-v} - \sqrt{v_{l-1}(1-v_l)/v_l}$ following DDIM solver, where $v_l = 1 - \sigma_{\text{diff}}^2(l)$.

The student model ϵ_{ϖ} is trained to fit the linear interpolation between $\mathbf{Z}_t^{(l)}$ and $\mathbf{Z}_t^{(l-1)}$, $\forall l \in \{1, 2, \dots, L\}$, by solving the following noise matching problem:

$$\min_{\varpi} \sum_{l=1}^L \mathbb{E}_{\mathbf{Z}_t^{(l)} \sim \varphi_l} \left[\int_{\tau_{l-1}}^{\tau_l} \left\| \frac{\mathbf{Z}_t^{(l-1)} - \vartheta_k \mathbf{Z}_t^{(l)}}{\varrho_l} - \epsilon_{\varpi}(\mathbf{Z}_t^{(\tau)}, \tau) \right\|^2 d\tau \right], \quad (13)$$

where $\mathbf{Z}_t^{(l-1)} = \Phi(\mathbf{Z}_t^{(l)}, \tau_l, \tau_{l-1}) \sim \varphi_{l-1}$, and $\mathbf{Z}_t^{(\tau)} = \frac{\tau - \tau_l}{\tau_l - \tau_{l-1}} \mathbf{Z}_t^{(l)} + \frac{\tau_l - \tau}{\tau_l - \tau_{l-1}} \mathbf{Z}_t^{(l-1)}$. The optimum of (13) can be given by $\epsilon_{\varpi}^*(\mathbf{Z}_t^{(\tau)}, \tau) = \mathbb{E} \left[\frac{\mathbf{Z}_t^{(l-1)} - \vartheta_k \mathbf{Z}_t^{(l)}}{\varrho_l} \middle| \mathbf{Z}_t^{(\tau)} \right]$. Therefore, the reconstruction loss to learn parameters ϖ can be given by

$$L_{\text{RF}} = \left\| \epsilon_{\varpi}(\mathbf{Z}_t^{(\tau)}, \tau) - \frac{\mathbf{Z}_t^{(l-1)} - \vartheta_k \mathbf{Z}_t^{(l)}}{\varrho_l} \right\|^2. \quad (14)$$

During offline distillation, we randomly sample the number of denoising steps $L \in \{1, 2, \dots, L_{\max}\}$ and the time point $\tau \in (\tau_{l-1}, \tau_l]$. Then, the few-step denoising diffusion model is trained by minimizing the reconstruction loss (14) to solve the noise matching problem. The distilled denoising diffuser can recursively obtain denoised features $\mathbf{Z}_t^{(L)}, \mathbf{Z}_t^{(L-1)}, \dots, \mathbf{Z}_t^{(0)}$ using (12). Therefore, the latent features extracted by ES-side sub-model $\mathcal{F}^E(\cdot)$ in time frame t can be given by $\mathbf{Z}_t^O = \mathbf{Z}_t^{(0)}$.

2) *Feature Merging for Length-Adaptive Compression*: As the feature transmissions are very crucial for collaborative generation at ES and UE, we propose a length-adaptive feature compression scheme in this part, which reduces the dimensions of transmitted features by merging similar neurons specific to different latent features \mathbf{Z}_t^O . It is worth noting that conventional pruning schemes inevitably incurs performance loss, since they completely discard the information of pruned neurons that are considered as less important. In comparison, we fuse the information of pruned features into the remaining neurons, thus enabling more efficient compression.

The length-adaptive feature compression is realized by dynamically merging the neurons that are output by the last U-Net blocks. These neurons are also known as tokens in the realms of large language model (LLM) and GAI, which is the most fundamental building blocks of Transformer layers. The idea of *token merging* has been recently proposed for Transformer or self-attention layer [24], [25]. However, current studies mainly focus on computation acceleration and the *token merging* ratio is predefined manually. To support length-adaptive feature compression, our proposed protocol involves a novel dynamic feature merging scheme, which flexibly reduces the neurons of transmitted features in the online radio environment. To realize this, we first introduce an offline distillation process for learning a backbone decoder at the UE. Given the randomly sampled feature merging ratios, the VAE decoder at the UE is trained to reconstruct high-quality images using the merged features received through noisy wireless channels.

Mathematically, the self-attention matrix $\mathbf{A}_t \in \mathbb{R}^{d^C \times d^V}$ of the Transformer layer in the last U-Net block is written as

$$\mathbf{A}_t = \text{softmax} \left(\frac{1}{\sqrt{d^K}} \mathbf{X}_t^U \mathbf{W}^Q (\mathbf{X}_t^U \mathbf{W}^K)^T \right) \mathbf{X}_t^U \mathbf{W}^V, \quad (15)$$

where $\mathbf{X}_t^U \in \mathbb{R}^{d^C \times d^F}$ denotes the input tokens of the last U-Net block, with d^C being the number of latent feature channels, and d^F denotes the numbers of input tokens. Moreover, $\mathbf{W}^K \in \mathbb{R}^{d^F \times d^K}$ and $\mathbf{W}^Q \in \mathbb{R}^{d^F \times d^K}$ denote the model weight for key and query matrices calculation, and $\mathbf{W}^V \in \mathbb{R}^{d^F \times d^V}$ signifies the model weight for value matrix calculation. Thus, the unmerged latent vector

\mathbf{Z}^O can be calculated by

$$\mathbf{Z}_t^O = \mathbf{A}_t * \mathbf{W}^{\text{CONV}} \in \mathbb{R}^{d^C \times d^W d^H}, \quad (16)$$

where \mathbf{W}^{CONV} denotes the 2D convolutional neural layer weights and $*$ is the convolutional operation. d^W and d^H indicate the width and height of latent features, and thus the maximum number of tokens for transmitted features can be given by $J_{\max} = d^W d^H$.

To compress latent features targets, $J_t = \lfloor \beta_t J_{\max} \rfloor$ useful tokens will be retained after merging. To determine which tokens need to be pruned and merged when the merging ratio β_t is given, we measure the similarity between different tokens, thus merging the output tokens tailored to real-time latent features and channel conditions. It is worth noting that the token merging needs to be performed via a fast procedure, which makes conventional iterative clustering method (e.g., K-means) computationally impractical. To this end, we consider a low-complexity solution here. Specifically, we calculate the cosine similarity $\Lambda_{m,m'}$ for any two tokens m and m' , $m' \geq m$, which can be defined as

$$\Lambda_{m,m',t} = \frac{\mathbf{z}_{m,t}^O \cdot \mathbf{z}_{m',t}^O}{\|\mathbf{z}_{m,t}^O\| \|\mathbf{z}_{m',t}^O\|}, \forall m, m' \in \{1, 2, \dots, M_{\max}\}. \quad (17)$$

Then, we merge the most similar $M_t = M_{\max} - \lfloor M_{\max} \alpha_t \rfloor$ pairs of tokens. As each merging operation reduces one token, we can finally meet the required ratio and reserve $\lfloor M_{\max} \alpha_t \rfloor$ tokens with lower similarities. Let $\Psi_{m,m',t}$ denote the binary indicator that denotes whether token m will be merged into token m' , i.e.,

$$\Psi_{m,m',t} = \begin{cases} 1, & \Lambda_{m,m',t} \text{ is the top-}M_t \text{ similarity score,} \\ 0, & \text{otherwise.} \end{cases} \quad (18)$$

By merging the similar tokens, the reserved token n can be updated by

$$\mathbf{z}_{n,t} = \frac{1}{\bar{\Psi}_{m,t} + 1} \left(\mathbf{z}_{m,t}^O + \sum_{n' \in \mathcal{N}} \mathbf{z}_{n',t}^O \right), \quad (19)$$

where $\bar{\Psi}_{m,t} = \sum_{m'} \Psi_{m,m',t}$.

Based on the above merging operation $\mathcal{F}^M(\cdot)$, we achieve the length-adaptive latent feature:

$$\mathbf{Z}_t = \mathcal{F}^M(\beta_t, \mathcal{F}^E(\alpha_t, \mathbf{X}_t)) \in \mathbb{R}^{d^C \times J_t}. \quad (20)$$

The UE then receives the noisy latent feature through the wireless channels, i.e.,

$$\widehat{\mathbf{Z}}_t = \mathbf{Z}_t + \mathbf{N}_t, \quad (21)$$

with Gaussian noises $\mathbf{N}_t \sim \mathcal{N}(0, \sigma^2)$. To keep the consistency of the feature decoder inputs, the UE further reconstructs the unmerged features $\widehat{\mathbf{Z}}_t$ by duplicating $\widehat{\mathbf{z}}_{m,t}$ to obtain $\widehat{\mathbf{z}}_{m',t}^O, \forall \Psi_{m,m',t} = 1$. Then, UE learns to decode the target images from the received noisy features by

$$\mathbf{Y}_t = \mathcal{F}^D(\beta_t, \widehat{\mathbf{Z}}_t). \quad (22)$$

During the offline distillation stage, the denoising diffuser and VAE decoder can be respectively trained at ES and UE to mitigate the reconstruction loss by randomly sampling the denoising steps and feature merging ratios. A backbone meta-architecture is then constructed, which will be utilized for dynamic compression in the online stage.

B. Dynamic MEG Acceleration as A Constrained MDP

Based on the meta-architecture trained via offline stage, the online dynamic acceleration can be further formulated as a constrained MDP model \mathcal{M}_C , which is defined as

$$\mathcal{M}_C = \left(\mathbf{s}_t, \mathbf{a}_t, \pi, P(\mathbf{s}_{t+1} | \mathbf{s}_t, \mathbf{a}_t), \gamma, R_t, C_t \right). \quad (23)$$

Specifically, at each time frame t , the dynamic compression predictor observes the environment states $\mathbf{s}_t = [h_t, \Omega_t, \Delta_{t-1}]$, which stacks the vectorized information of instantaneous CSI, UEs' computation backlogs, and the previous frame duration. The dynamic feature merging ratios and denoising steps can be predicted by the policy π_θ , which is parameterized by θ . According to system observations at each time frame t , the dynamic compression predictor samples the action from the policy π_θ , i.e.,

$$\mathbf{a}_t = [\alpha_t, \beta_t] \sim \pi_\theta(h_t, \Omega_t, \Delta_{t-1}). \quad (24)$$

Then, the length-adaptive features \mathbf{Z}_t can be further extracted by feature merging $\mathcal{F}^M(\cdot)$ using (20). Therefore, the generated content \mathbf{Y}_t is jointly inferred by the learning-based policy $\pi(\cdot | \mathbf{s}_t)$, the feature merging $\mathcal{F}^M(\cdot)$, and the feature encoder/decoder $\mathcal{F}^E(\cdot)$ and $\mathcal{F}^D(\cdot)$. Mathematically, the generated high-resolution images using the designed protocol can be modelled by

$$\mathbf{Y}_t = \pi_\theta(\alpha_t, \beta_t | \mathbf{s}_t) \mathcal{F}^D(\mathcal{F}^M(\beta_t, \mathcal{F}^E(\alpha_t, \mathbf{X}_t)), \mathbf{N}_t). \quad (25)$$

Afterwards, the reward function $R_t = F_G(\mathbf{Y}_t, \mathbf{a}_t | \mathbf{s}_t)$ indicates the resulting image generation qualities and can be measured from the environment feedback. Then, the state transits from \mathbf{s}_t to \mathbf{s}_{t+1} under the action \mathbf{a}_t , as specified by the state transition probability $P(\mathbf{s}_{t+1} | \mathbf{s}_t, \mathbf{a}_t)$. Therefore, our goal is transformed to maximize the discounted returns $G^R = \mathbb{E}_{\rho \sim \pi} \left[\sum_{t=0}^{\infty} \gamma^t R(\mathbf{s}_t, \mathbf{a}_t) \right]$ with discount factor $\gamma \in [0, 1]$, while limiting the costs of energy and latency constraint violations to a threshold $\varepsilon \in [0, +\infty]$, i.e.,

$$\mathcal{P}_{\text{CMDP}} : \max_{\pi} G^R(\pi), \quad (26a)$$

$$\text{s.t. C3}, \quad (26b)$$

$$\text{C4} : G_i^C(\pi) \leq \varepsilon_i, \quad \forall i \in \{1, 2\}, \quad \forall t \in \mathcal{T}, \quad (26c)$$

where C3 can be achieved by projecting the output variables into ranges $[0, 1]$, and the original latency and energy consumption constraints C1 and C2 are recast as C4. Moreover, $G_i^C(\pi) = \mathbb{E}_{\rho \sim \pi} \left[\sum_{t=0}^{\infty} \gamma^t C_{t,i} \right]$ denotes the discounted expected costs, where $C_{t,i}$, $i \in \{1, 2\}$, indicates the violations of constraints C1 and C2, respectively.

IV. CONSTRAINED REINFORCEMENT LEARNING FOR ONLINE MEG ACCELERATION

A. Overview of Constrained Reinforcement Learning

In this section, we address the resulting constrained MDP for online MEG acceleration based on RL. To achieve higher image quality while guaranteeing both latency and energy constraints, we commence by revisiting the conventional Lagrangian-based method [27], and then introduce the constrained variational policy optimization (CVPO) theory [28] to achieve more efficient constraint guarantees for online prediction.

1) *Conventional Lagrangian-based Method:* We first introduce the conventional Lagrangian-based method that is commonly adopted in solving constrained MDP. The main principle is to transfer the constrained MDP problem $\mathcal{P}_{\text{CMDP}}$ into a min-max optimization problem:

$$(\pi^*, \boldsymbol{\lambda}^*) = \arg \min_{\lambda \geq 0} \max_{\pi} G^R(\pi_{\theta}) - \lambda_i (G_i^C(\pi_{\theta}) - \varepsilon_i), \quad (27)$$

where $\boldsymbol{\lambda} = [\lambda_1, \lambda_2]$ denotes the Lagrange multiplier vector and λ_i , $i = 1, 2$, is the non-negative Lagrange multiplier (i.e., dual variable) corresponding to constraint C6. The constrained MDP can be addressed by alternatively improving policy parameters of π_{θ} and updating Lagrange multipliers to iteratively solve the min-max problem. Note that selecting the appropriate dual

variable is crucial for constraint guarantees, which should satisfy $\lambda_i \rightarrow +\infty$ when $G_i^C > \varepsilon_i$ and $\lambda_i = 0$ when $G_i^C \leq \varepsilon_i$. Solving $\mathcal{P}_{\text{CMDP}}$ approximately leads to suboptimal dual variables. Furthermore, due to the non-stationary cost penalty terms, the primal problem is hard to optimize via the policy gradients backpropagated from multiple Q-value functions.

2) *Variational Policy Optimization Method*: To overcome the above issues, the constrained MDP for dynamic MEG acceleration can be transformed into a probabilistic variational inference problem. First, we define a variable O to represent the event of optimal reward maximization. For an infinite discounted reward, the likelihood of reward maximization given a trajectory ρ is proportional to the exponential of the discounted cumulative reward, which can be written as

$$\log \Pr(O = 1 | \rho) \propto \exp\left(\frac{\sum_t \gamma^t R_t}{\kappa}\right), \quad (28)$$

where κ denotes the temperature parameter. Let $p_\pi(\rho)$ denote the probability of obtaining a trajectory ρ under the policy π . Thus, the log-likelihood of optimality under the policy π has the following lower bound:

$$\log p_\pi(O = 1) = \log \int \Pr(O = 1 | \rho) p_\pi(\rho) d\rho \geq \mathcal{U}(q, \pi), \quad (29)$$

where $\mathcal{U}(q, \pi)$ denotes the evidence lower bound (ELBO), defined as

$$\mathcal{U}(q, \pi) \triangleq \mathbb{E}_{\rho \sim q} \left[\sum_{t=0}^{\infty} \gamma^t R_t \right] - \kappa D_{\text{KL}}(q(\rho) \| p_\pi(\rho)). \quad (30)$$

Furthermore, $p_\pi(\rho)$ denotes the actual action distribution generated by policy π , and $q(\rho)$ is an auxiliary action distribution that approximates $p_\pi(\rho)$ while satisfying the constraints. More specifically, $p_\pi(\rho)$ and $q(\rho)$ can be defined as

$$\begin{aligned} p_\pi(\rho) &= p(\mathbf{s}_0) \prod_{t \geq 0} P(\mathbf{s}_{t+1} | \mathbf{s}_t, \mathbf{a}_t) \pi(\mathbf{a}_t | \mathbf{s}_t) P(\boldsymbol{\theta}), \\ q(\rho) &= p(\mathbf{s}_0) \prod_{t \geq 0} P(\mathbf{s}_{t+1} | \mathbf{s}_t, \mathbf{a}_t) q(\mathbf{a}_t | \mathbf{s}_t), \quad \forall q \in \Pi_q, \end{aligned} \quad (31)$$

where Π_q represents the set of feasible action distribution subject to constraints C_i , which is given by

$$\Pi_q = \left\{ q(\mathbf{a} | \mathbf{s}) : G_i^C(q) < \varepsilon_i, i \in \{1, 2\}, \mathbf{a} \in \mathcal{A}, \mathbf{s} \in \mathcal{S} \right\}, \quad (32)$$

with $G_i^C(q) = \mathbb{E}_{\rho \sim q} [\sum_{t=0}^{\infty} \gamma^t C_{t,i}]$, $i \in \{1, 2\}$, being the discounted expected cost under probability distribution q . Substituting the above definitions into (30), we can obtain that

$$\mathcal{U}(q, \pi) = \mathbb{E}_{\rho \sim q} \left[\sum_{t=0}^{\infty} (\gamma^t R_t - \kappa D_{\text{KL}}(q(\cdot | \mathbf{s}_t) \| \pi(\cdot | \mathbf{s}_t))) \right] + \kappa \log P(\boldsymbol{\theta}), \quad \forall q(\mathbf{a} | \mathbf{s}_t) \in \Pi_q. \quad (33)$$

CVPO alternates between the Expectation step (E-step) and the Maximization step (M-step) for constrained policy learning. Specifically, the E-step optimizes the lower bound $\mathcal{U}(q, \pi)$ with respect to q within the feasible action distribution set Π_q . Furthermore, the M-step optimizes the policy parameters π within the parameter space $\pi \in \Pi$. The above expectation-maximization (EM) procedure decouples the inaccurate dual variable optimization and the policy improvement, and bridge these two components via a variational distribution. The main difficulty turns into searching for the variational distribution within the constrained set. Fortunately, the constrained q distribution can be solved analytically with optimality and feasibility guarantee through convex optimization. In the following part, we will develop the constrained MEG policy learning algorithm by combining the convex optimization and the supervised learning.

B. MEG-CVPO Algorithm Design

1) *E-Step Optimization*: In each training iteration n , the E-step aims to search for the optimal variational distribution $q \in \Pi_q$, which guarantees the constraints whilst improving expected returns. Given the sampled trajectory $\rho = \{(\mathbf{s}_t, \mathbf{a}_t, R_t)\}_{t=1}^T$ from the replay buffer, the goal is to optimize the following KL objective obtained from (33):

$$\mathcal{P}_E : \max_q \mathcal{U}(q, \pi) = \mathbb{E}_{\mathbf{s} \sim \psi_q} [\mathbb{E}_{\rho \sim q} [Q_n^R(\mathbf{s}, \mathbf{a})] - \kappa D_{\text{KL}}(q \| \pi_n)], \quad (34a)$$

$$\text{s.t. C3}, \quad (34b)$$

$$\text{C5} : \mathbb{E}_{\mathbf{s} \sim \psi_q} [\mathbb{E}_{\rho \sim q} [Q_{i,n}^C(\mathbf{s}, \mathbf{a})]] \leq \varepsilon_i, \quad \forall i \in \{1, 2\}, \quad (34c)$$

where constraint C4 is rewritten into C5, ψ_q denotes the stationary state distribution based on current variational distribution, and the reward value Q_n^R and the cost value $Q_{i,n}^C$ are defined as

$$Q_n^R = \mathbb{E}_{\rho \in \pi_n, \mathbf{s}_0 = \mathbf{s}, \mathbf{a}_0 = \mathbf{a}} \left[\sum_{t=0}^{\infty} \gamma^t R_t \right], \quad (35)$$

$$Q_{i,n}^C = \mathbb{E}_{\rho \in \pi_n, \mathbf{s}_0 = \mathbf{s}, \mathbf{a}_0 = \mathbf{a}} \left[\sum_{t=0}^{\infty} \gamma^t C_{t,i} \right]. \quad (36)$$

Therefore, Q_n^R and $Q_{i,n}^C$ are estimated by the sampled trajectory $\rho \sim \pi_n$. Constraint C5 guarantees that the optimized variational distribution q lies within the feasible set Π_q . Problem \mathcal{P}_E can be viewed as a constrained KL-regularized optimization problem. To avoid tuning the penalty coefficient κ in the regularized term, we can further introduce a hard regularization constraint as follows:

$$\tilde{\mathcal{P}}_E : \max_q \tilde{\mathcal{U}}(q) = \mathbb{E}_{\mathbf{s} \sim \psi_q} \left[\int q(\mathbf{a} | \mathbf{s}) Q_n^R(\mathbf{s}, \mathbf{a}) d\mathbf{a} \right], \quad (37a)$$

$$\text{s.t. C5 : } \mathbb{E}_{\mathbf{s} \sim \psi_q} \left[\int q(\mathbf{a} | \mathbf{s}) Q_{i,n}^C(\mathbf{s}, \mathbf{a}) d\mathbf{a} \right] \leq \varepsilon_i, \quad \forall i \in \{1, 2\}, \quad (37b)$$

$$\text{C6 : } \mathbb{E}_{\mathbf{s} \sim \psi_q} [D_{\text{KL}}(q \| \pi_n)] \leq \varepsilon_0, \quad (37c)$$

$$\text{C7 : } \int q(\mathbf{a} | \mathbf{s}) d\mathbf{a} = 1, \quad \forall \mathbf{s} \in \psi_q, \quad (37d)$$

where C5 is the cost constraint rearranged from (34c), C6 is the regularization constraint that limits the variational distribution q within a trust region of the policy distribution at the n -th training iteration, and C7 ensures that the variational distribution q leads to valid actions across all the states.

By regarding $q(\mathbf{a} | \mathbf{s})$ as a optimization variable instead of a parameterized function, problem $\tilde{\mathcal{U}}(q)$ becomes a convex optimization problem. The Lagrangian function of the constrained E-step optimization problem can be written as

$$\begin{aligned} \mathcal{L}_\lambda(q, \zeta, \boldsymbol{\lambda}, \xi) = & \int \psi_q(\mathbf{s}) \int q(\mathbf{a} | \mathbf{s}) Q_n^R(\mathbf{s}, \mathbf{a}) d\mathbf{a} d\mathbf{s} + \sum_i \lambda_i \left(\varepsilon_i - \int \psi_q(\mathbf{s}) \int q(\mathbf{a} | \mathbf{s}) Q_{i,n}^C(\mathbf{s}, \mathbf{a}) d\mathbf{a} d\mathbf{s} \right) \\ & + \zeta \left(\varepsilon_0 - \int \psi_q(\mathbf{s}) \int q(\mathbf{a} | \mathbf{s}) \log \frac{q(\mathbf{a} | \mathbf{s})}{\pi_n(\mathbf{a} | \mathbf{s})} d\mathbf{a} d\mathbf{s} \right) + \xi \left(1 - \int \psi_q(\mathbf{s}) \int q(\mathbf{a} | \mathbf{s}) d\mathbf{a} d\mathbf{s} \right), \end{aligned} \quad (38)$$

where $\boldsymbol{\lambda}$, ζ , and ξ denote the Lagrangian multipliers for constraints C7 – C9. Then, the dual problem is given by

$$\min_{\zeta, \boldsymbol{\lambda}, \xi} \max_q \mathcal{L}_\lambda(q, \zeta, \boldsymbol{\lambda}, \xi). \quad (39)$$

The derivative of \mathcal{L}_λ with respect to q can be given by

$$\frac{\partial \mathcal{L}_\lambda}{\partial q} = Q_n^R(\mathbf{s}, \mathbf{a}) - \sum_i \lambda_i Q_{i,n}^C - \zeta \left(1 + \log \frac{q(\mathbf{a} | \mathbf{s})}{\pi_n(\mathbf{a} | \mathbf{s})} \right) - \xi. \quad (40)$$

Using the first-order optimality, i.e., $\frac{\partial \mathcal{L}_\lambda}{\partial q} = 0$, the optimal variational distribution within Π_q for

problem $\tilde{\mathcal{P}}_E$ is given by

$$q^*(\mathbf{a} | \mathbf{s}) = \frac{\pi_n(\mathbf{a} | \mathbf{s})}{A_n} \exp\left(\frac{\tilde{Q}_n(\mathbf{s}, \mathbf{a})}{\zeta}\right), \quad (41)$$

where $A_n = \exp(1 + \xi/\zeta)$ means the constant normalizer for the optimized distribution q , and $\tilde{Q}_n(\mathbf{s}, \mathbf{a})$ is defined as

$$\tilde{Q}_n(\mathbf{s}, \mathbf{a}) = Q_n^R(\mathbf{s}, \mathbf{a}) - \sum_i \lambda_i Q_{i,n}^C(\mathbf{s}, \mathbf{a}). \quad (42)$$

Substituting (41) into (38) and ignoring irrelevant terms, the optimal dual variables ζ^* and $\boldsymbol{\lambda}^*$ can be obtained by optimizing the unconstrained convex problem

$$\min_{\zeta, \boldsymbol{\lambda} \geq 0} F(\zeta, \boldsymbol{\lambda}), \quad (43)$$

where $F(\zeta, \boldsymbol{\lambda})$ is the Lagrangian function given by

$$F(\zeta, \boldsymbol{\lambda}) = \sum_i \lambda_i \varepsilon_i + \zeta \varepsilon_0 + \zeta \mathbb{E}_{\mathbf{s} \sim \psi_q} \left[\log \mathbb{E}_{\mathbf{a} \sim \pi_n} \left[\exp\left(\frac{\tilde{Q}_n(\mathbf{s}, \mathbf{a})}{\zeta}\right) \right] \right]. \quad (44)$$

This unconstrained convex problem can be easily solved by performing gradient descent updates over ζ and $\boldsymbol{\lambda}$, given by

$$\zeta \leftarrow \zeta - \nu_\zeta \frac{\partial F(\zeta, \boldsymbol{\lambda})}{\partial \zeta}, \quad \boldsymbol{\lambda} \leftarrow \boldsymbol{\lambda} - \nu_\lambda \frac{\partial F(\zeta, \boldsymbol{\lambda})}{\partial \boldsymbol{\lambda}}, \quad (45)$$

where ν_λ and ν_ζ denote the learning rates for dual variables $\boldsymbol{\lambda}$ and ζ , respectively.

2) *M-Step Optimization*: After obtaining an optimal feasible variational distribution q_n^* from the E-step optimization, the M-step further maximizes the ELBO to update the policy $\pi_\theta = \pi(\mathbf{a}_t | \mathbf{s}_t)$, where $\boldsymbol{\theta}$ denotes the learnable policy parameters. Ignoring irrelevant terms in (33) with respect to $\boldsymbol{\theta}$, the M-step solves the following posterior maximization problem

$$\max_{\boldsymbol{\theta}} \int \psi_q(\mathbf{s}) \int q^*(\mathbf{a} | \mathbf{s}) \log \pi_\theta(\mathbf{a} | \mathbf{s}) d\mathbf{a} d\mathbf{s} + \log P(\boldsymbol{\theta}), \quad (46)$$

To compute $P(\boldsymbol{\theta})$, we sample the M-step policy parameters around the old policy parameters $\boldsymbol{\theta}_n$ with a Gaussian prior regularizer, i.e., $\boldsymbol{\theta} \sim \mathcal{N}\left(\boldsymbol{\theta}_n, \frac{F_\theta}{\mu}\right)$, with Σ_θ being the Fisher information matrix and μ being a positive constant coefficient. Based on the Gaussian prior, the log-prior can be written as

$$\log P(\boldsymbol{\theta}) = -\mu (\boldsymbol{\theta} - \boldsymbol{\theta}_n)^T \Sigma_\theta^{-1} (\boldsymbol{\theta} - \boldsymbol{\theta}_n) \stackrel{(a)}{\geq} -\mu D_{\text{KL}}(\pi_n || \pi_\theta), \quad (47)$$

Algorithm 1 Training Procedure of MEG-CVPO Algorithm

Input: Constrained RL batch size B_{RL} , particle size K , numbers of gradient update iterations I_{E} and I_{M} for E-step and M-step.

Output: Constrained policy parameters θ .

- 1: Initialize policy parameters θ_0 .
- 2: **for** each iteration $n = 1, 2, \dots$ **do**
 - 3: **for** each batch execution epoch **do**
 - 4: Sample α_t and β_t according to policy π_n by observing \mathbf{s}_t at each time frame t .
 - 5: ES extracts feature \mathbf{Z}_t using sub-model $\mathcal{F}^{\text{E}}(\alpha_t, \mathbf{X}_t)$.
 - 6: ES calculates the similarity using (17), and merge the feature via (18) - (19).
 - 7: UE receives feature $\widehat{\mathbf{Z}}_t$ from the ES under \mathbf{N}_t , unmerges the received features, and decodes \mathbf{Y}_t by sub-model $\mathcal{F}^{\text{D}}(\cdot)$.
 - 8: Evaluate the generation quality and update replay buffer by the collected transitions.
 - 9: **end for**
 - 10: */** Perform E-step policy optimization*
 - 11: Sample a set of \mathcal{B}_n transitions.
 - 12: Update Q_n^{R} and $Q_{i,n}^{\text{C}}$, $i \in \{1, 2\}$, by Bellman backup.
 - 13: **for** each batch $b = 1, 2, \dots, B_{\text{RL}}$ **do**
 - 14: Sample K actions $\mathbf{a}_1, \mathbf{a}_2, \dots, \mathbf{a}_K$ for current state \mathbf{s}_n .
 - 15: Calculate $Q_n^{\text{R}}(\mathbf{s}_n, \mathbf{a}_k)$ and $Q_{i,n}^{\text{C}}(\mathbf{s}_n, \mathbf{a}_k)$, $\forall k$.
 - 16: **end for**
 - 17: Update dual variable ζ and λ via (45) for I_{E} iterations to solve (44).
 - 18: Update the variational distribution for state $\mathbf{s} \in \mathcal{B}_n$ using (41).
 - 19: */** Perform M-step policy optimization*
 - 20: Update policy parameters θ_n via (51) for I_{M} iterations.
 - 21: **end for**

where (a) can be obtained by second-order Taylor expansion of $D_{\text{KL}}(\pi_n \parallel \pi_\theta)$. Therefore, the M-step objective function can be transferred into maximizing the tight lower bound

$$\max_{\theta} \int \psi_q(\mathbf{s}) \int (q^*(\mathbf{a} \mid \mathbf{s}) \log \pi_\theta(\mathbf{a} \mid \mathbf{s}) d\mathbf{a} - \mu D_{\text{KL}}(\pi_n \parallel \pi_\theta)) d\mathbf{s}. \quad (48)$$

Similar to E-step, to eliminate the hyperparameter μ , we can transform the above soft regularized KL term into the hard KL constraint $D_{\text{KL}}(\pi_n \parallel \pi_\theta) \leq \tilde{\varepsilon}$. This leads to the following M-step Lagrangian function

$$\mathcal{L}_\lambda(\theta, \vartheta) = \int \psi_q(\mathbf{s}) \int q^*(\mathbf{a} \mid \mathbf{s}) \log \pi_\theta(\mathbf{a} \mid \mathbf{s}) d\mathbf{a} d\mathbf{s} + \vartheta (\tilde{\varepsilon} - C_\theta), \quad (49)$$

with $C_\theta \triangleq (\theta - \theta_n)^T F_\theta^{-1} (\theta - \theta_n)$ and ϑ being the dual variable for hard KL constraint. Therefore, the dual problem is given by

$$\max_{\theta} \min_{\vartheta} \mathcal{L}_\lambda(\theta, \vartheta). \quad (50)$$

Based on gradient descent, the policy parameters can be updated by

$$\boldsymbol{\theta} \leftarrow \boldsymbol{\theta} + \nu_{\theta} \frac{\partial \mathcal{L}_{\lambda}(\boldsymbol{\theta}, \vartheta)}{\partial \boldsymbol{\theta}}, \quad \vartheta \leftarrow \vartheta - \nu_{\vartheta} \frac{\partial \mathcal{L}_{\lambda}(\boldsymbol{\theta}, \vartheta)}{\partial \vartheta}, \quad (51)$$

where ν_{θ} and ν_{ϑ} denote the learning rates. For ease of implementation, the integral operation is replaced by summation by sampling K particles in the continuous action space. The training procedure of MEG-CVPO algorithm can be summarized in **Algorithm 1**.

V. NUMERICAL RESULTS: A CASE STUDY OF *SDXL* ACCELERATION

A. Experimental Setup

To present the performance, we focus on the case studies for dynamic acceleration of *Stable Diffusion XL (SDXL)* [29], which is a large-scale LDM extensively applied in a broad range of GAI applications, e.g., text-to-image generation, image editing/synthesis, and music generation. *SDXL* surpasses the behaviour performance of all previous stable diffusion (SD) models with 3x larger U-Net blocks and advanced conditioning scheme. While *SDXL* is capable of generating high-resolution images (typically 1024×1024 pixels), the intensive attention blocks in U-Net backbone and the increased latent feature sizes results in extraordinarily unaffordable computation burdens to directly perform it at mobile terminals.

TABLE I: Simulation parameters

Parameter	Value	Parameter	Value
Radius	300 [m]	Computing efficiency	$f^{\text{ES}} = 1/0.0274$ [TFLOPS]
Pathloss	$35.3 + 37 \cdot \log(\text{dist}[\text{m}])$ [dB]	Energy efficiency	$f^{\text{UE}} = 0.5 f^{\text{ES}}$ [TFLOPS]
AWGN N_0	-107 dBm	FLOPs of VAE encoder	$f^{\text{ES}} = 1/0.0774$ [hJ/TFLOPs]
Bandwidth	1 [MHz]	FLOPs of single U-Net block	$f^{\text{UE}} = 0.8 f^{\text{ES}}$ [hJ/TFLOPs]
Size of latent feature	$(d^{\text{C}}, d^{\text{W}}, d^{\text{H}}) = (16, 64, 64)$	FLOPs of VAE decoder	$O^{\text{E}} = 0.2200$ [TFLOPs]
Size of action particles	$K = 32$		$O^{\text{UNet}} = 11.2482$ [TFLOPs]
Learning rate	$\nu_{\zeta} = \nu_{\lambda} = 0.02, \nu_{\theta} = 0.0005$		$O^{\text{D}} = 10.2310$ [TFLOPs]

For feature transmissions of MEG, we set the transmitting power at BS at $P_0 = 15$ dBm, and the channel bandwidth allocated to the UE is 1 MHz. For decoding images from the received features over the noisy channels, the peak signal-to-noise ratio (PSNR) is given by $\frac{P_0}{\sigma^2} = 0$ dB. We collect a subset of high-resolution images from LAIONON-COCO-Aesthetic dataset [30] with 20000 training samples and 2000 test samples. The image quality is evaluated by calculating the mean square error (MSE) between the generated images and the reference images, where the reference image is generated by the centralized *SDXL* scheme with $L_{\text{max}} = 12$ and transmitted

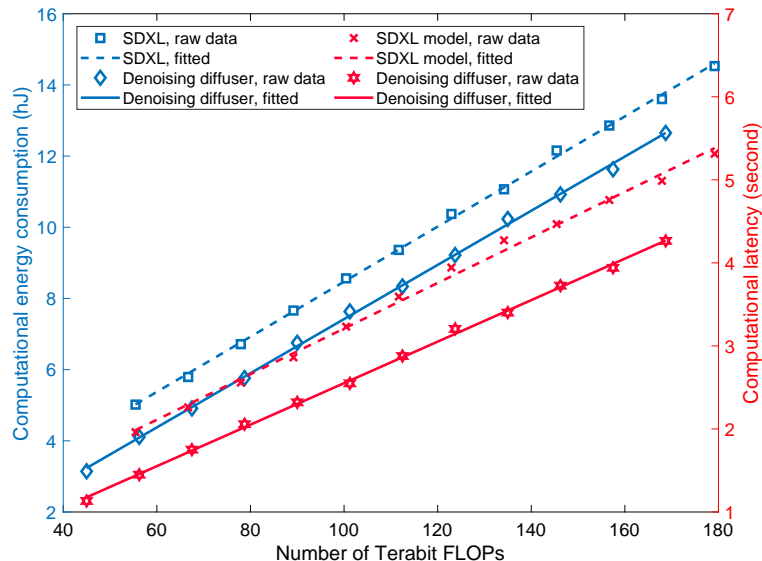


Fig. 3: Latency and energy consumption models of the proposed MEG framework.

through perfect channels. Each floating point number takes up 16 bits during both computations and transmissions. Based on the measurement results in a Linux workstation with 2 Nvidia A40 GPUs and PyTorch, both realistic latency and energy consumption are linearly related to FLOPs, as shown in Fig. 3. This validates the soundness of the considered latency and energy consumption models. The corresponding simulation parameters can be summarized in Table I.

To verify the performance of the proposed framework, we introduce the following baselines.

- **Centralized Generation** (perfect channels): The centralized *SDXL* model is deployed at the ES, which takes $L_{\max} = 12$ denoising steps. The generated 1024×1024 colour images will be transmitted to the UE through the perfect channels.
- **MEG-Split**: The pretrained *SDXL* model is directly split into two parts and deployed at the ES and UE without finetuning and feature compression.
- **MEG-Split-Finetune**: The split *SDXL* sub-models are deployed at the ES and UE, and the decoder is fine-tuned over noisy channels to minimize MSE for distortion mitigation.
- **MEG-Pruning**: Based on the split *SDXL* sub-models, a pruning-based adaptive feature encoder scheme similar to [13] is utilized, which can dynamically compress transmitted features in the online channel environment.
- **MEG-PPO-Lagrangian**: The Lagrangian-based constrained learning method is utilized for online prediction of MEG, which is integrated into the proximal policy optimization (PPO) framework [31]. To enhance the dual variable update stability of the vanilla Lagrangian-based method, the proportional and derivative (PID) control is also considered [32].

To ensure fairness, a pretrained few-step denoiser diffuser is enabled at all baselines. To further

accelerate computations for *MEG-Pruning* and our proposed MEG scheme, we also implement the *token merging* at each self-attention layer with a merging ratio $\tilde{\beta} = 0.5$.

B. Performance Evaluation



Fig. 4: Images created by different generation methods. The text prompt is given by “Two people standing in the snow with skis”.

1) *Offline Distillation Performance*: Exploiting the proposed dynamic diffusion and feature merging scheme, we train the meta-architecture of distributed sub-models via offline distillation. Given the same prompt, Fig. 4 compares the image samples generated by different models. The detailed numerical results have been presented in Table II. As shown in Fig. 4(b), the *MEG-Split* scheme generates highly noisy images. As an advance, *MEG-Split-Finetune* can overcome the channel noises and generates high-fidelity images, but still requires a relatively high latency. In contrast, *MEG-Pruning* can further reduce the computation and transmission latencies, but leads to inevitable distortion since the pruning forces some image details to be missing. Based

TABLE II: Detailed numerical result comparison of different methods. $L_{\max} = 12$.

Method Performance	Centralized Generation (Perfect channels, $L = 12$)	<i>MEG-Split</i> ($L = 8$)	<i>MEG-Split-Finetune</i> ($L = 8$)	<i>MEG-Pruning</i> ($L = 8, \beta = 0.1$)	MEG (proposed) ($L = 8, \beta = 0.5$)	MEG (proposed) ($L = 4, \beta = 0.5$)
MSE	0 (Reference)	0.2842	0.0106	0.0153	0.0095	0.0246
Transmission latency (second)	82.51	1.7189	1.7189	1.5470	0.9132	0.9132
Computation latency (second)	7.5806	5.2122	5.2122	3.2316	3.2316	2.0287

on feature merging, our proposed MEG scheme can reduce over 90% and over 40% latency compared to the centralized generation and *MEG-Split-Finetune* schemes, respectively, while generating meaningful high-resolution images and retain sufficient image details.

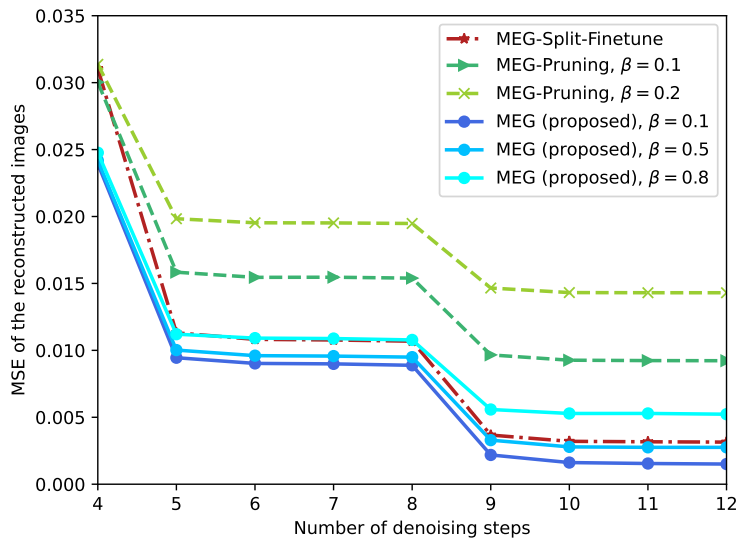
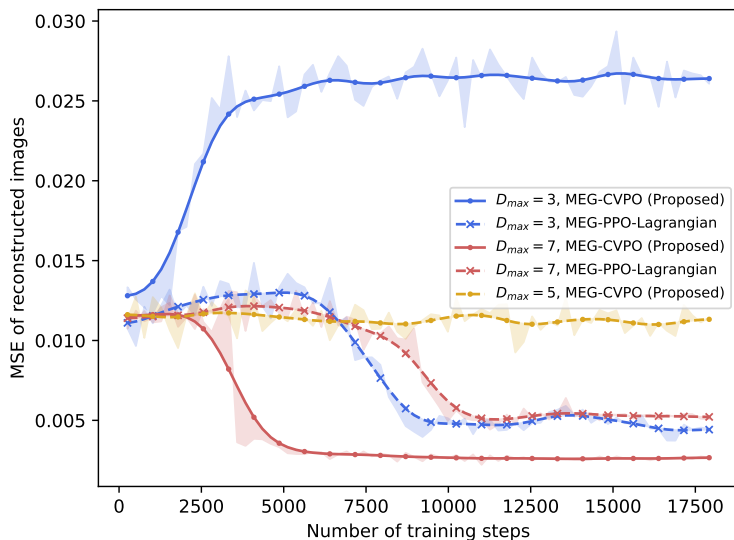


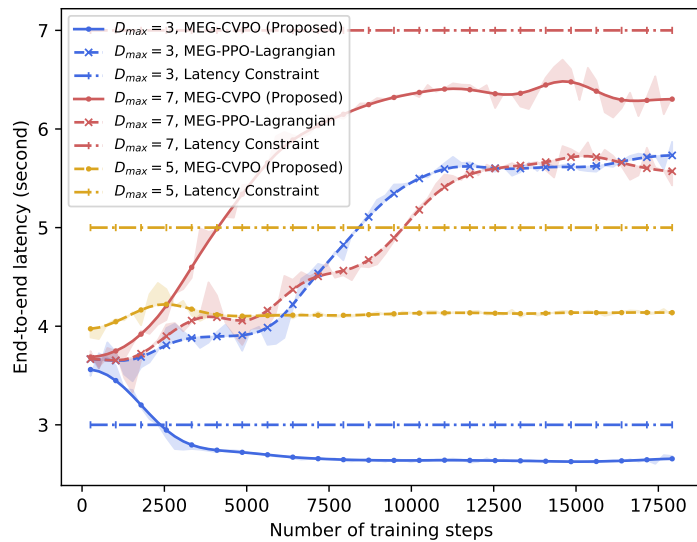
Fig. 5: Comparisons of average MSE achieved by different generation scheme.

Fig. 5 demonstrates the performance of the proposed framework under configurations of different denoising steps and feature compression ratios. The MSE decreases with denoising steps and increases with feature compression ratios, which confirms the trade-off between the image generation quality and costs. It can be observed that the *MEG-Pruning* scheme results in a much higher MSE than *MEG-Split-Finetune* scheme, even when the pruning ratio is low. In comparison, the proposed dynamic feature merging scheme can achieve high generation qualities comparable to *MEG-Split-Finetune* when merging ratio $\beta = 0.5$, and outperforms *MEG-Split-Finetune* even when merging ratio $\beta = 0.8$. This verifies the feature compression efficiency of the proposed scheme for distributed image generations. It is worth noting that the proposed scheme may outperform *MEG-Split-Finetune* especially when the denoising step is small, which implies that training with merged features may enhance the noise resistance performance of the UE decoder.

2) *Constrained Learning Performance*: We further validate the constrained learning performance of the proposed MEG-CVPO algorithm for online prediction. The batch size for policy learning is set as 64. We train both MEG-CVPO and *MEG-PPO-Lagrangian* algorithms in 70 epochs, and utilize the Adam optimizer for gradient descent. Fig. 6 presents the average MSE



(a)



(b)

Fig. 6: Performance comparisons of constrained learning algorithms in the test stage. $E_{\max} = 1.8$ kJ. (a) Average MSE of the generated images. (b) Performance of latency constraint guarantees.

and latency guarantee performance for different constrained learning algorithms. Both MEG-CVPO and *MEG-PPO-Lagrangian* can converge within 15000 training steps. As shown in Fig. 6(a), when the maximum latency requirement is relaxed (i.e., $D_{\max} = 7$ seconds), MEG-CVPO can achieve a higher generation quality compared to *MEG-PPO-Lagrangian*, which verifies its efficiency in optimizing denoising steps and feature merging ratios. Both MEG-CVPO and *MEG-PPO-Lagrangian* can guarantee the latency constraints in this case, as demonstrated in Fig. 6(b). However, when a low latency is required (i.e., $D_{\max} = 3$ seconds), MEG-CVPO

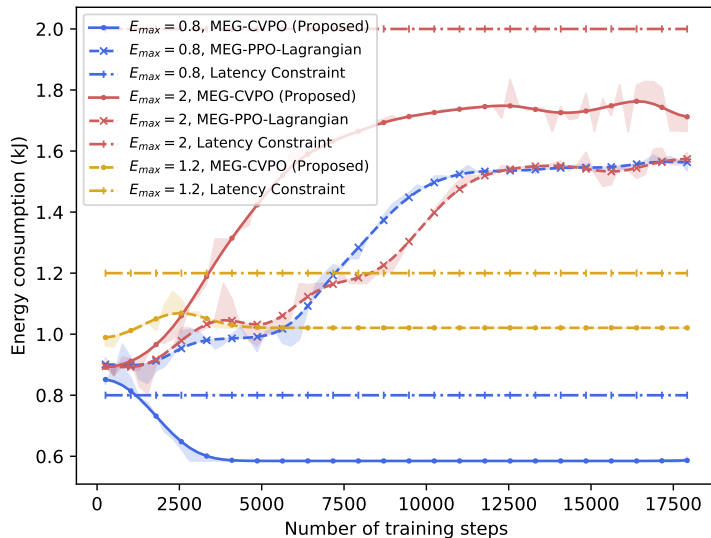


Fig. 7: Performance comparisons of energy constraint guarantees. $D_{\max} = 8$ seconds.

leads to a much higher MSE than *MEG-PPO-Lagrangian*, since the budgets of computational and transmission overheads are significantly reduced. As a result, the proposed MEG-CVPO algorithm can still stringently guarantee the latency constraint, while *MEG-PPO-Lagrangian* suffering obvious constraint violations. Furthermore, the proposed MEG-CVPO algorithm can also adaptively adjust the dynamic denoising steps and feature merging ratios to strictly satisfy a latency requirement of $D_{\max} = 5$ seconds, which will yield a compromised image quality. This also demonstrates that the proposed MEG-CVPO algorithm can realize a controllable quality-latency trade-off for on-device image generation.

Fig. 7 further compares the energy consumptions of different algorithms under different energy budgets. The *MEG-PPO-Lagrangian* algorithm severely violates the energy consumption constraint when the energy budget is small. In contrast, by optimizing the feasible action distributions and learning policies in the corresponding trusted regions, the proposed MEG-CVPO algorithm can strictly satisfy various energy consumption requirements. In addition, the gap between the energy consumption of MEG-CVPO and the specified energy budget is tighter compared to that of *MEG-PPO-Lagrangian*. This also indicates that MEG-CVPO can improve the efficiency of resource utilization in resource-constrained systems.

VI. CONCLUSION

A novel accelerated mobile edge generation (MEG) framework has been proposed to enable cost-efficient AIGC services at edge networks. Leveraging the decomposed LDM sub-models distributed across the ES and the UE, the proposed framework achieves on-device high-resolution

image generation with low transmission and computing overheads. The denoising steps and feature merging ratio were jointly optimized, aiming to maximize the image generation quality while satisfying latency and energy consumption constraints. To address this optimization problem and tailor the LDM sub-models for dynamic acceleration, we developed a low-complexity dynamic acceleration MEG protocol. More specifically, a backbone meta-architecture has been trained via offline distillation. Then, the dynamic diffusion and feature merging were realized in an online channel environment, which can be modelled as a constrained MDP. An MEG-CVPO algorithm has been further developed, which effectively trained the policy to enhance image quality and ensure feasible action distributions. Numerical results revealed the efficiency of the proposed framework in accelerating high-resolution image generation and resisting distortions. Additionally, the proposed MEG-CVPO algorithm can effectively ensure constraints and adaptively balance between generation quality and costs. For the future outlook, practical and scalable edge resource management can be further explored by extending the proposed framework into parallel and multi-user AIGC applications.

REFERENCES

- [1] O. AI, "Chatgpt: Optimizing language models for dialogue," "Accessed Jun. 30, 2024", [Online]. Available: <https://openai.com/blog/chatgpt/>.
- [2] O. AI, "DALL-E 3," <https://openai.com/index/dall-e-3/>, [Online]. Available: <https://openai.com/index/dall-e-3/>.
- [3] S. Huang, P. Grady, and GPT-3, "GenerativeAI: A creative new world," "Accessed Jun. 30, 2024", [Online]. Available: <https://www.sequoiacap.com/article/generative-AI-a-creative-new-world/>.
- [4] M. Xu et al., "Unleashing the Power of Edge-Cloud Generative AI in Mobile Networks: A Survey of AIGC Services," *IEEE Commun. Surveys Tut.*, vol. 26, no. 2, pp. 1127-1170, Secondquarter 2024.
- [5] R. Cheng, Y. Sun, D. Niyato, L. Zhang, L. Zhang, and M. A. Imran, "A Wireless AI-Generated Content (AIGC) Provisioning Framework Empowered by Semantic Communication," *arXiv preprint arXiv: 2310.17705*, 2024.
- [6] H. Cai, C. Gan, T. Wang, Z. Zhang, and S. Han, "Once-for-all: Train one network and specialize it for efficient deployment," in *Proc. Int. Conf. Learn. Represent.*, Addis Ababa, Ethiopia, Apr. 2020.
- [7] R. Zhong, X. Mu, Y. Zhang, M. Jabor, and Y. Liu, "Mobile Edge Generation: A New Era to 6G," *arXiv preprint arXiv: 2401.08662*, 2024.
- [8] E. Li, Z. Zhou, and X. Chen, "Edge intelligence: On-demand deep learning model co-inference with device-edge synergy," in *Proc. Workshop Mobile Edge Commun., Budapest*, Hungary, Aug. 2018, pp. 31-36.
- [9] Y. Shi, K. Yang, T. Jiang, J. Zhang, and K. B. Letaief, "Communication-efficient edge AI: Algorithms and systems," *IEEE Commun. Surveys Tuts.*, vol. 22, no. 4, pp. 2167-2191, 4th Quart., 2020.
- [10] E. Li, Z. Zhou, and X. Chen, "Edge intelligence: On-demand deep learning model co-inference with device-edge synergy," in *Proc. Workshop Mobile Edge Commun., Budapest*, Hungary, Aug. 2018, pp. 31-36.
- [11] Y. Kang, J. Hauswald, C. Gao, A. Rovinski, T. Mudge, J. Mars, and L. Tang, "Neurosurgeon: Collaborative intelligence between the cloud and mobile edge," *ACM SIGARCH Comput. Archit. News*, vol. 45, no. 1, pp. 615-629, Apr. 2017.

- [12] H. Li, C. Hu, J. Jiang, Z. Wang, Y. Wen, and W. Zhu, "JALAD: Joint accuracy-and latency-aware deep structure decoupling for edge-cloud execution," in *Proc. Int. Conf. Parallel Distrib. Syst.*, Singapore, Dec. 2018, pp. 671-678.
- [13] J. Shao, Y. Mao and J. Zhang, "Learning Task-Oriented Communication for Edge Inference: An Information Bottleneck Approach," *IEEE J. Sel. Areas Commun.*, vol. 40, no. 1, pp. 197-211, Jan. 2022.
- [14] N. Tishby, F. C. Pereira and W. Bialek, "The information bottleneck method," *Proc. Annu. Allerton Conf. Commun. Control Comput.*, pp. 368-377, Oct. 1999.
- [15] J. Shao and J. Zhang, "Bottlenet++: An end-to-end approach for feature compression in device-edge co-inference systems," in *Proc. Int. Conf. Commun. Workshop*, Dublin, Ireland, Jun. 2020, pp. 1-6.
- [16] X. Xu, R. Zhong, X. Mu, Y. Liu, K. Huang, "Mobile Edge Generation-Enabled Digital Twin: Architecture Design and Research Opportunities," *arXiv preprint arXiv: 2407.02804*, 2024.
- [17] H. Du, R. Zhang, D. Niyato, J. Kang, Z. Xiong, D. I. Kim, X. Shen, and H. V. Poor, "User-Centric Interactive AI for Distributed Diffusion Model-based AI-Generated Content," *arXiv preprint arXiv: 2311.11094*, 2023.
- [18] J. Wang, H. Du, D. Niyato, J. Kang, Z. Xiong, D. Rajan, S. Mao et al., "A Unified Framework for Guiding Generative AI with Wireless Perception in Resource Constrained Mobile Edge Networks," *arXiv preprint arXiv:2309.01426*, 2023.
- [19] S. Li, Xi Lin, Y. Liu, and J. Li, "Trustworthy AI-Generative Content in Intelligent 6G Network: Adversarial, Privacy, and Fairness", *arXiv preprint arXiv: 2405.05930*, 2024.
- [20] O. Ronneberger, P. Fischer, and T. Brox, "U-Net: Convolutional Networks for Biomedical Image Segmentation," *arXiv preprint arXiv:1505.04597*, 2015.
- [21] C. Meng, Y. Song, J. Song, J. Wu, J. Zhu, and S. Ermon. "SDEdit: Guided Image Synthesis and Editing with Stochastic Differential Equations," *arXiv preprint, arXiv:2108.01073*, 2021.
- [22] J. Song, C. Meng, and S. Ermon, "Denoising Diffusion Implicit Models," *arXiv preprint, arXiv:2010.02502*, June 2022.
- [23] R. Desislavov, et al., "Compute and energy consumption trends in deep learning inference," *arXiv preprint arXiv:2109.05472*, 2021.
- [24] D. Bolya, C. Fu, X. Dai, P. Zhang, C. Feichtenhofer, and J. Hoffman, "Token Merging: Your ViT But Faster," in *Proc. Int. Conf. Learn. Represent.*, 2023.
- [25] D. Bolya, J. Hoffman, "Token Merging for Fast Stable Diffusion," in *Proc. IEEE/CVF Conf. Comput. Vis. Pattern Recognit. (CVPR)*, 2023, pp. 4599-4603.
- [26] H. Yan, X. Liu, J. Pan, J. H. Liew, Q. Liu, and J. Feng, "Perflow: Piecewise rectified flow as universal plug-and-play accelerator", *arXiv preprint arXiv:2405.07510*, May 2024.
- [27] D. Ding, k. Zhang, t. Basar, and M. Jovanovic, "Natural policy gradient primal-dual method for constrained markov decision processes," in *Proc. Adv. Neural Inf. Process. Syst.*, pp. 8378-8390, 2020.
- [28] Z. Liu, Z. Cen, V. Isenbaev, W. Liu, S. Wu, B. Li, and D. Zhao, "Constrained Variational Policy Optimization for Safe Reinforcement Learning," in *Proc. Int. Conf. Mach. Learn.*, pp. 13644-13668, 2022.
- [29] D. Podell, Z. English, K. Lacey, A. Blattmann, T. Dockhorn, J. Muller, J. Penna, and R. Rombach, "SDXL: Improving latent diffusion models for high-resolution image synthesis," *arXiv preprint arXiv:2307.01952*, 2023.
- [30] C. Schuhmann, R. Beaumont, R. Vencu, C. Gordon, R. Wightman, M. Cherti, T. Coombes, A. Katta, C. Mullis, M. Wortsman, et al. "Laion-5b: An open large-scale dataset for training next generation image-text models," *Proc. Adv. Neural Inf. Process. Syst.*, pp. 25278-25294, 2022.
- [31] J. Schulman, F. Wolski, P. Dhariwal, A. Radford, and O. Klimov. "Proximal policy optimization algorithms," *arXiv preprint arXiv:1707.06347*, 2017.
- [32] A. Stooke, J. Achiam, and P. Abbeel, "Responsive safety in reinforcement learning by pid lagrangian methods," in *Int. Conf. Mach. Learn.*, pp. 9133-9143, 2020.